ORIGINAL ARTICLE

Examination of *Cinnamomum camphora* interlocked grain adopting X-ray computed tomography combined with particle image velocimetry

Hairi Cipta, Kayoko Kobayashi, Shuoye Chen and Junji Sugiyama*

Abstract

Trees develop wood grain more or less parallel to the tree axis as they grow laterally. However, many tree species also develop interlocked grain that is expressed as a change in the wood grain orientation, periodically switching between left- and right-handed spirals over the years. Wood grain information is critical to determining the wood quality and is an important record of cellular events in a cambium. This study examined the wood grain of axial xylem cells in the semi-ring porous hardwood *Cinnamomum camphora* by first visualizing the three-dimensional structure using a conventional X-ray computed tomography instrument producing tomography images. We propose the use of particle image velocimetry (PIV) and the two-dimensional fast Fourier transform (2D-FFT) to analyze computed tomography images in obtaining grain angle (δ) information from the vessel deviation. We found undulation on the radial variation of the grain angle (δ) that indicates periodical changes in the wood grain orientation as left- and right-handed spirals ranging from $-25°$ to $16°$ and $-22°$ to $18°$ using the 2D-FFT and PIV, respectively. Furthermore, despite the major orientation of vessels inclining in the tangential direction, the PIV result revealed a minor deviation with vessels inclining in various orientations along the tree radius.

Keywords: Grain angle, Image analysis, Tracking algorithm, Vessel network, Water transport

Introduction

The wood grain of a living tree is not always straight or parallel to the longitudinal axis of the tree [1]. Terms have been used to define the inclined grain depending on the degree of deviation from the longitudinal axis: namely, wavy grain, spiral grain, and interlocked grain [1, 2]. An interlocked grain occurs when there is a periodic change in the grain angle between left- to right-handed spirals over the course of years [3–5]. Such grain deviation affects the woodworking process and physical–mechanical properties of the wood [1, 6–8].

The interlocked grain of tropical tree species has been reported in numerous studies [4, 6, 9–14]. In the present study, we observed the interlocked grain of *Cinnamomum camphora,* which usually grows in temperate and subtropical regions [15–17]. *Cinnamomum camphora* wood is selected for making Buddhist images and cabinets in Japan [18]. Unlike the case for tropical species, which have a less clear growth ring boundary, the growth ring boundary of *C. camphora* is annual and distinct because the earlywood vessels appear to be distinctly larger than latewood vessels. Such type of vessel porosity is known as semi-ring porous.

The wood grain orientation is related to the orientation of longitudinal cells that reflect the orientation of parental fusiform cambial cells [1–3, 11, 19, 20]. Therefore, in addition to using the conventional radial splitting

*Correspondence: sugiyama.junji.6m@kyoto-u.ac.jp

Graduate School of Agriculture, Kyoto University, Sakyo-Ku, Kyoto 606-8502, Japan

Cipta *et al. Journal of Wood Science* (2022) 68:56

Page 2 of 10

method, which is invasive [3, 6, 9], wood grain orientation can be evaluated by examining the orientation of longitudinal cells such as fibers and vessels. Fibers generally account for 30–80% on composition of angiosperm wood, by volume, which will define grain orientation. To see fibers at the cellular level and evaluate grain orientation, serial sectioning on tangential sections is commonly used [11].

Vessels also originate from the same parental cells as fibers. Thus, vessel orientation can also be used as a proxy for grain orientation [4, 11, 19, 21, 22]. Although the vessels and fibers have similar orientation, different grain orientations commonly occur in reversal zone of interlocked grain in which vessels run steeper than fibers [13, 21, 22]. Unlike fibers, vessels are actually long hollow tubes that can extend from centimeters to meters in length that have relatively larger diameters. These vessels are composed of longitudinally aligned series of vessel elements [23]. We can take advantage of this structure for examining grain orientation. The orientation can be measured by mapping vessels on consecutive transverse sections [24]. When vessels are inclined and not parallel to the longitudinal axis of the tree, there is a lateral shift of the vessel between two consecutive transverse sections at different depths. However, serial sectioning technique is time-consuming, requiring training and experience to obtain a satisfactory result. Meanwhile, cross-correlation has been adopted to automatically evaluate the grain angle from such lateral shifting in a pair of transverse images from different depths extracted from a single cross section using a confocal microscope [13]. However, this method only works on pair transverse images with narrow depth because of the inadequate intensity of the lower image of the section. Additionally, this method requires sectioning of the sample.

X-ray computed tomography (CT) has been applied in wood science studies in recent decades to observe the spatial organization of xylem, which is usually obtained through time-consuming serial sectioning [25]. The CT technique allows the virtual cutting of a wood sample simulating microtomy, including obtaining serial transverse sections and other sections from any surface. The technology allows a wider region to be observed in a single image acquisition of the wood sample with relatively faster processing compared to serial sectioning method. It also provides a clear surface because X-ray attenuation addresses the problem of the inadequate intensity of the lower image when adopting confocal microscopy. In addition, interlocked grain of two African mahogany species [22] and spiral grain of radiata pine [26] have been studied recently using high-resolution CT. These studies make use of CT technique capacity to reconstruct 3D view of wood at cellular level.

Depending on the equipment, a varied resolution of CT images might be obtained [27]. Ideally, we can select the equipment based on the requirement of the investigation. However, in certain situations, we are unable to employ a CT equipment with high-resolution imaging. Meanwhile, with lower resolution CT images, it is difficult to visualize wood elements at the cellular level, especially fibers which are important to examine grain orientation. Nevertheless, due to their larger size, vessels can still be observed in lower resolution CT images. For example, we have previously used considerably lower resolution CT imaging at 50 μm/pixel and found enough to detect vessels in *C. camphora* [28]. Therefore, we sought to develop a technique that can evaluate the orientation based on appearance of vessels on lower resolution CT images.

We propose adopting particle image velocimetry (PIV) to evaluate the interlocked grain of transverse images of *C. camphora* wood. PIV is often used to study liquid or gas material flow, cell imaging, and cloud motion among other applications [29–32]. We adopt PIV to evaluate the grain deviation in pairs of CT images of *C. camphora* transverse sections by tracking the possibility of displacement of vessels and other cells as particle-like objects in image pairs with different depths. This analysis involves dividing the images into several sub-regions and applying cross-correlation across image pairs [33]. In addition, the two-dimensional fast Fourier transform (2D-FFT) [11, 13, 22] is used to evaluate the interlocked grain in the tangential section. The present paper shows the possibility of evaluating the grain orientation from *C. camphora* images recorded using a low-resolution industrial X-ray CT machine by performing image analysis. We estimate the grain angle variation by applying PIV to transverse sections. The result of the PIV of transverse sections was then validated using the 2D-FFT of tangential sections. Furthermore, we demonstrate how the variation in the vessel orientation intra-annual ring can be obtained from the PIV output.

Materials and methods
Wood material
The wood block of *C. camphora* was similar to a block that was used in a previous study [28]. The block used in the present study was scanned using an X-ray CT instrument (Y.CT Modular, YXLON International GmbH, Hamburg, Germany) at the Kyushu National Museum. The CT scanning was conducted with a resolution of 0.05 mm per pixel. This process provided projection images, which were then reconstructed into two-dimensional (2D) image slices of the wood block. We used volume graphic software (VGStudio MAX 2.2, Volume Graphic GmbH, Heidelberg, Germany) to visualize the three-dimensional (3D) reconstructed volume of *C.*

Cipta *et al. Journal of Wood Science* (2022) 68:56

Page 3 of 10

camphora from the slices of 2D images and prepared a suitable image series for analysis.

Pretreatment

Images of a transverse section of the actual wood block were precisely prepared by aligning the volume of reconstructed CT images (Fig. 1). This process provided a series of transverse images with dimensions of 1433×1478 pixels. The images were rotated to align the annual rings in the vertical direction. The images were cropped to 948×344 pixels, corresponding to dimensions of 47.4 mm $\times$ 17.2 mm.

We prepared other datasets by extracting oblique transverse sections from a similar volume with the same dimensions as the transverse sections. Two types of oblique transverse section deviating in the tangential direction were prepared. The deviations were 10° in the clockwise direction and 10° in the counterclockwise direction relative to the longitudinal axis of the tree.

Tangential images of the same scale were prepared from a similar volume (Fig. 2a). A series of tangential images with dimensions of 1433×1001 pixels were generated. We then cropped the images to 427×491 pixels, corresponding to 21.35 mm $\times$ 24.55 mm.

Evaluation of the interlocked grain and vessel network through PIV

To measure interlocked grain, we extracted 36 sequential transverse images from the serial transversal images, where images were spaced at intervals of 10 pixels (500 μm). For each image, the next sequential image was its pairing image. A total of 35 pairs of transverse images were thus analyzed in the study. Each pair of images was analyzed adopting PIV. The PIV analysis was programmed in Python [34] using the OpenPIV package [35, 36]. The program splits each image into sub-regions. These sub-regions are called interrogation windows in the first image and search windows in the second image. We used a sub-region of 16×16 pixels for the interrogation window and a larger sub-region of 32×32 pixels for the search window. The sub-regions, either interrogation windows or search windows, overlapped each other at a distance of eight pixels from the center of the sub-region.

The PIV program provides a displacement vector of elements within the pair of images by demonstrating cross-correlation of the windows using the fast Fourier transform (FFT) function and statistical analysis to validate the vectors. The program tracks the most feasible displacement of elements in the sub-region that are assumed to be related to the wood grain orientation
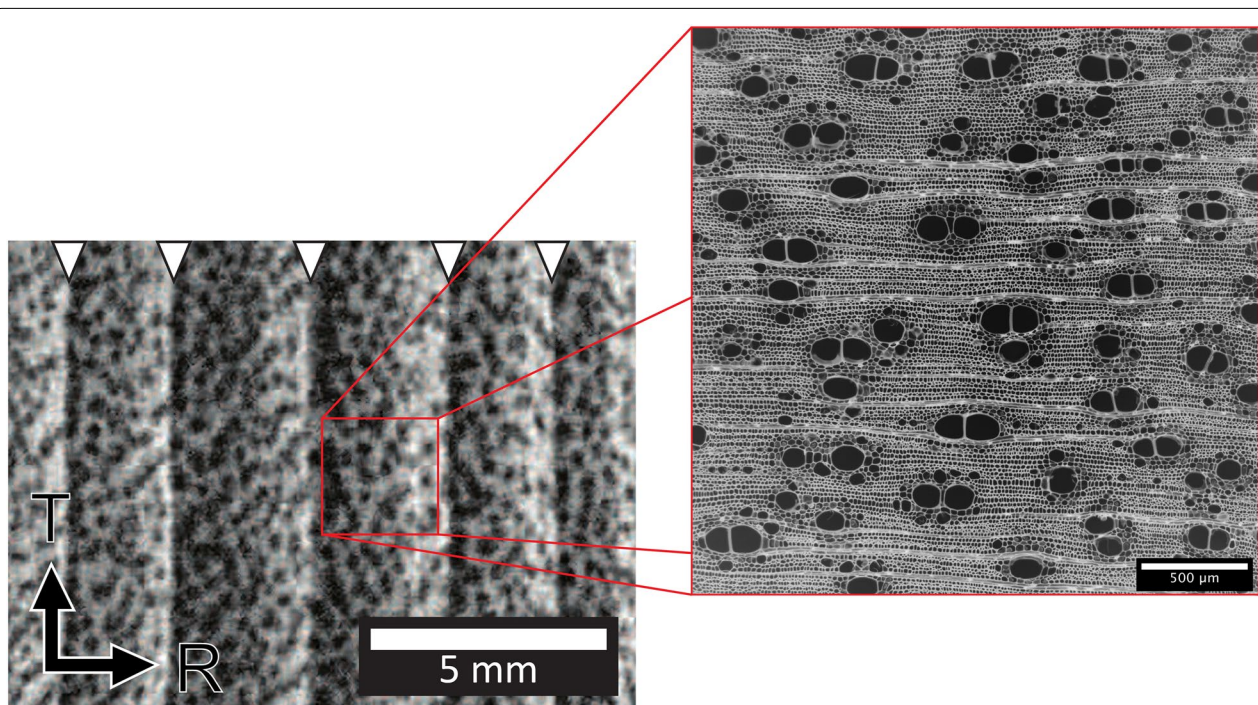

Fig. 1 Left: part of a transverse section of a CT image of *C. camphora* used in the present paper. Right: optical microscopy image of *C. camphora* anatomical features for a different specimen. White arrowheads indicate annual ring boundaries (left). The optical microscopy image (right) is inverted from a brightfield microscopy image to get similar black and white pattern with CT image
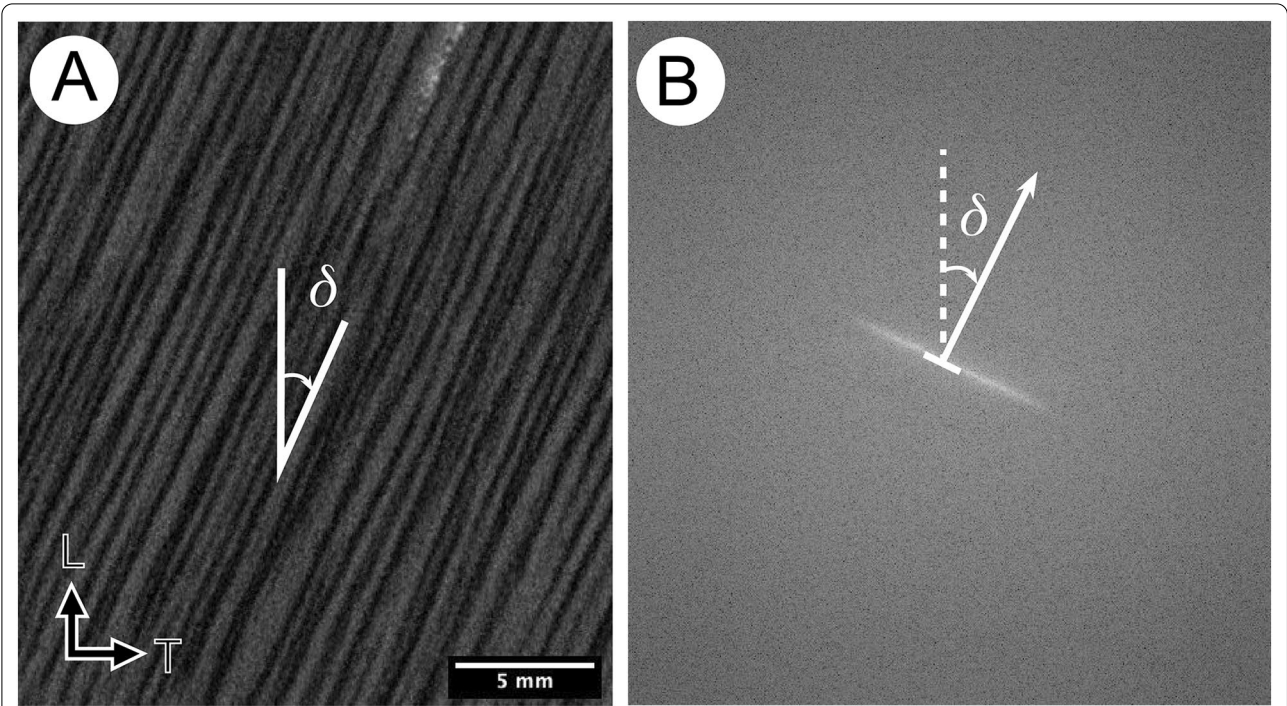
Fig. 2 a Tangential section of CT images showing an estimation of the *C. camphora* grain angle (*δ*). **b** Power spectrum, calculated from **a**, where the arrow indicates the grain angle (*δ*) measurement
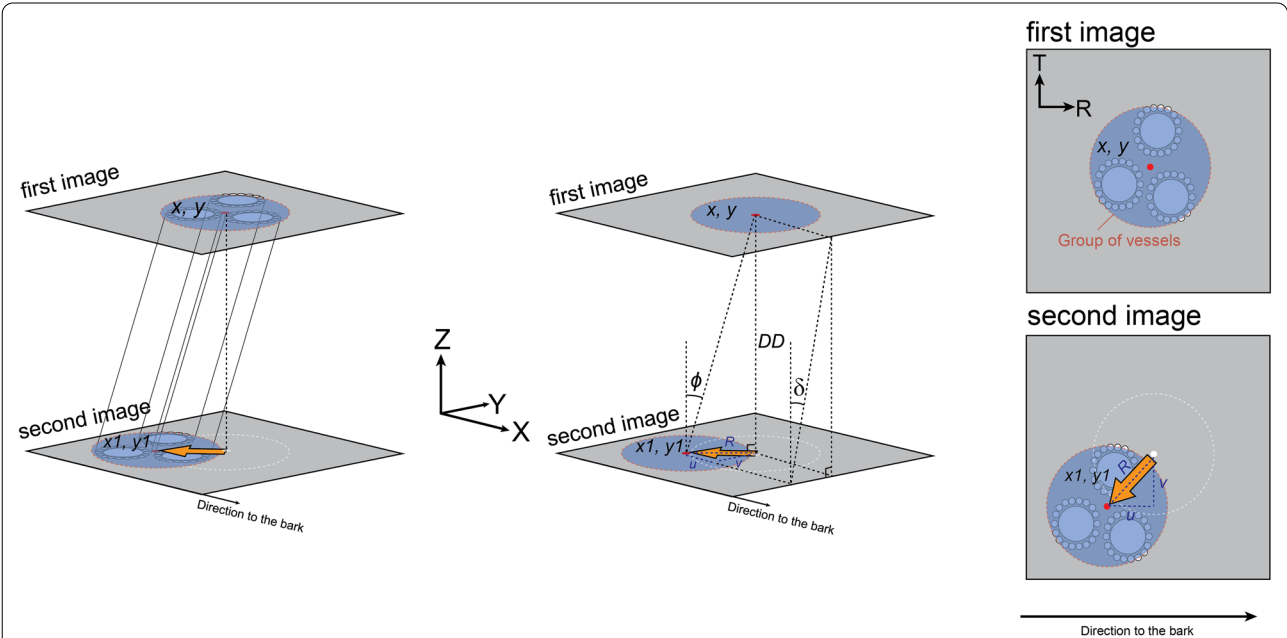

Fig. 3 Illustration of the lateral shifting of a group of vessels in two consecutive transverse images showing the definitions of the grain angle (*δ*) and inclination angle (*φ*). Coordinates *x, y* refer to the group of vessels in the first image whereas × *1, y1* refer to the most similar group in the second image. Wood orthotropic directions: tangential (X), radial (Y), and longitudinal (Z)

based on the movement of a group of vessels in two consecutive images, as illustrated in Fig. 3.

The output of the image analysis adopting PIV is the coordinates of sub-region vectors (x, y) and the vector displacement (u, v). Values u and v correspond to the deviation of the sub-region representing the grain inclination in radial and tangential directions, respectively. We measure the grain angle (δ) according to the displacement of a group of vessels with respect to the axial direction on the tangential plane as seen from the bark side. To obtain the grain angle (δ), we adapt an equation proposed by Ogata and Fujita [13] for examining the grain angle (δ) of *Hopea odorata* Roxb.:

$$\text{grain angle}(\delta) = tan^{-1}\left(\frac{v}{DD}\right), \tag{1}$$

where DD is the depth difference in pixels in the longitudinal direction between two consecutive images used for the measurement. A positive value corresponds to right-handed spiral grain and a negative value to left-handed grain. The variation in the radial grain angle obtained from PIV is measured by averaging the grain angle for 35 pairs of transverse images arranged in the longitudinal

direction. The value of the grain angle is then also averaged in the tangential direction.

The value of the grain angle (δ) is limited because it only gives the inclination of the grain in the tangential plane. We present another calculation from the PIV output, as illustrated in Fig. 3, to show the displacement vector of grain on a transverse surface representing the grain orientation and the inclination angle (ϕ) at the given orientation. The inclination angle (ϕ) represents the tilt of the grain from the direction of axial growth (Eq. 2). We use

$$\text{inclination angle}(\phi) = \tan^{-1}(\frac{R}{DD}), \tag{2}$$

$$R = \sqrt{u^2 + v^2}, \tag{3}$$

where R (Eq. 3) is the magnitude of the displacement and DD is the depth distance of the virtual sections.

Interlocked grain analysis using the 2D-FFT

We evaluated the grain angle (δ) from a series of tangential images and conducted 2D-FFT analysis by measuring
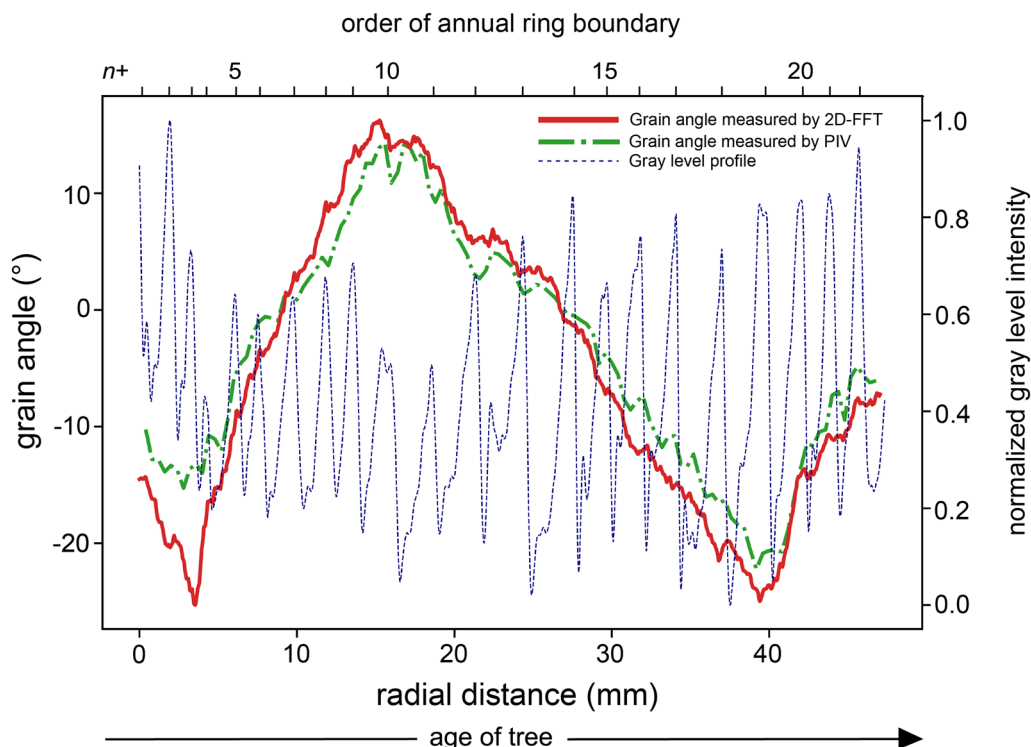

Fig. 4 Radial variation of the grain angle (δ) measured using PIV and 2D-FFT methods with a positive value indicating right-handed spirals grain and a negative value left-handed spirals grain as seen from the bark side. A dashed blue line represents the gray level profile along the radial direction with higher intensity correlating to higher density. The peaks represent the position of latewood that delineates annual rings

Cipta *et al. Journal of Wood Science*   (2022) 68:56

Page 6 of 10

the dominant orientation of streaks from the tangential images. The grain angle (δ) was evaluated from the tangential images automatically using the 2D-FFT algorithm provided in the Directionality plug-in for Fiji (http://fiji.sc/Fiji, Ashburn, VA) [22, 37, 38]. This program generated a power spectrum (Fig. 2b) with a streak representing the dominant grain orientation from a tangential image (Fig. 2a). The program then transformed the power spectrum into a histogram. The highest peak in the histogram was used to determine the grain angle (δ).

Results and discussion

Information on the anatomical structure from CT data

We present the analysis of the interlocked grain applying the PIV and 2D-FFT methods to CT images of *C. camphora*. Figure 1 shows the CT image and optical micrograph of *C. camphora* for a transverse section. Compared with the optical micrograph, the CT image with a resolution of 0.05 mm per pixel was unable to reproduce the detailed shape of xylem cells. However, we could recognize the vessel and surrounding cell lumen distribution as dark dots with a diffuse arrangement on the transverse plane. As expected, the differences in density between the vessel lumen and other cell tissue provided contrast sufficient to support further image analysis. Vessels are used as markers because they can be considered as particles in a transverse section for PIV analysis. We could also determine annual ring boundary based on radial density variation (Fig. 1). Abrupt changes of gray levels from bright to dark, indicating a transition between the end latewood zone into new earlywood zone, become the boundary between annual rings. Meanwhile, within annual ring, a part with brighter pixel is the earlywood part, and another part with darker pixel is the latewood part. However, we could not exactly demarcate the border between earlywood and latewood within annual rings. Moreover, we could see the vessel network as dark streaks on tangential planes that undergo periodical changes in orientation along the radial direction (Fig. 2a). Therefore, in the case of *C. camphora*, vessel elements could be important features in predicting the grain angle (δ) through X-ray CT.

Extracting 2D images from 3D volume CT observations mimics conventional serial sectioning without physically cutting the object. The serial section of the transverse plane of *C. camphora* shows vessels, implying that the continuity of vessel networks could deviate to a certain degree rather than follow a straight course (Additional file 1: Fig. S1). As seen in the present study, PIV is a useful image analysis tool with which to analyze the existence of interlocked grain in transverse images by tracking the displacement of the vessel network at different depths in
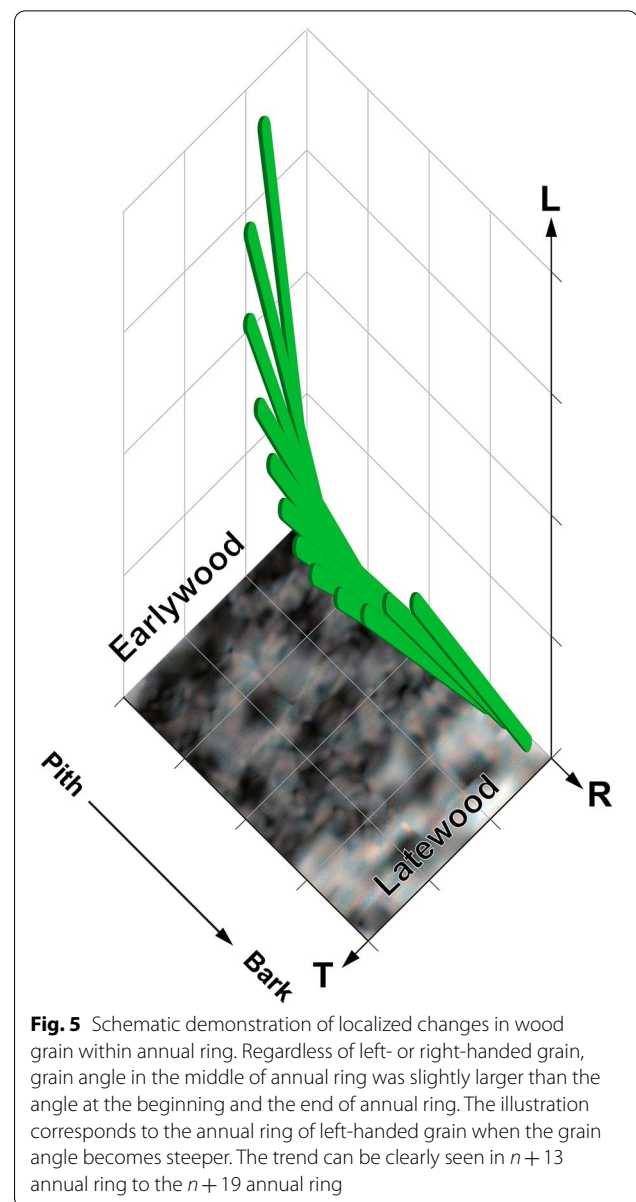

Fig. 5 Schematic demonstration of localized changes in wood grain within annual ring. Regardless of left- or right-handed grain, grain angle in the middle of annual ring was slightly larger than the angle at the beginning and the end of annual ring. The illustration corresponds to the annual ring of left-handed grain when the grain angle becomes steeper. The trend can be clearly seen in $n+13$ annual ring to the $n+19$ annual ring

the longitudinal direction. Meanwhile, serial sections on the tangential plane explicitly show a periodical change in the grain angle according to the vessel network alignment (Additional file 2: Fig. S2). Therefore, the 2D-FFT is a suitable option for evaluating the grain angle (δ) as exhibited by the arrangement of longitudinal elements on different tangential surfaces as performed in previous works on *Khaya ivorensis*, *K. senegalensis*, *Hopea odorata* and *Acacia mangium* [11, 13, 22].

The advantage of adopting X-ray CT is that we can perform virtual cutting at any surface position on a wood block. We can obtain transverse and tangential sections from a similar CT volume as demonstrated in this study.
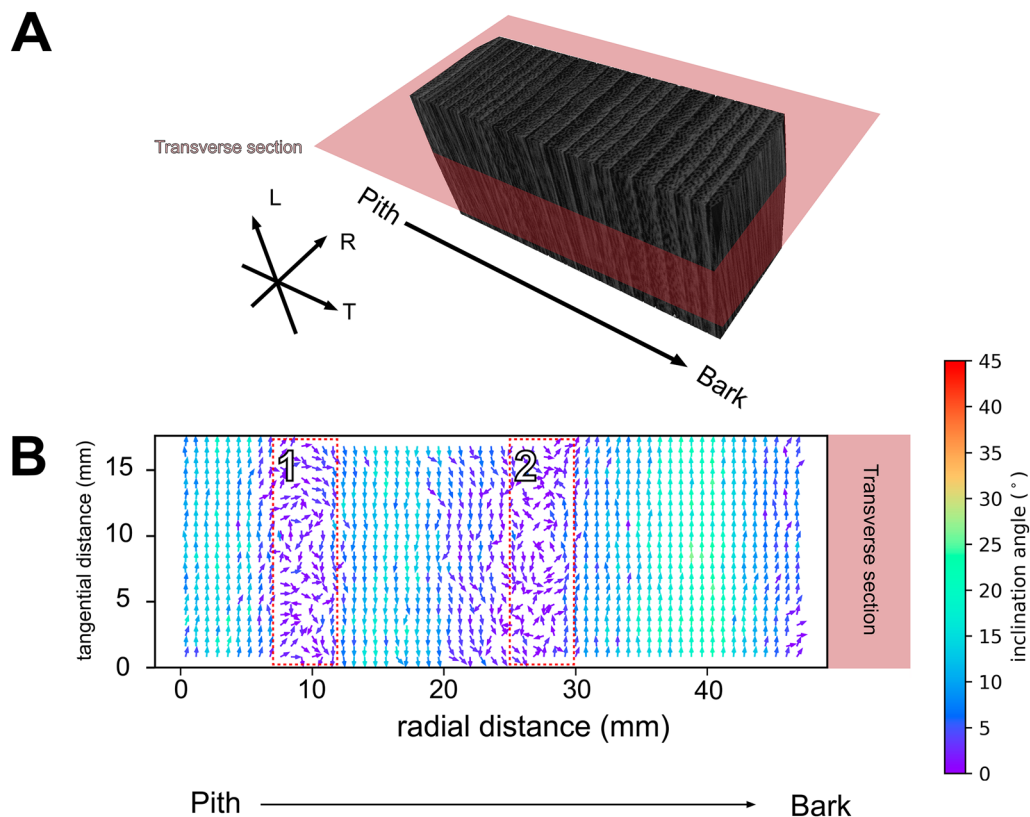
Cipta *et al. Journal of Wood Science* (2022) 68:56

Page 7 of 10

Fig. 6 a Illustration of the transverse section extracted from a *C. camphora* volume. **b** A visualization of the PIV output as a vector field representing the inclining orientation of vessels from an example pair of consecutive transverse images. The arrow color indicates the inclination angle (*φ*) according to the color bar. Zones 1 and 2 are dominated by nearly straight-oriented vessels with an inclination angle 0°–5°. Not all vectors are displayed to avoid overplotting

We can even provide other datasets for other sections, such as the oblique transverse section. Additionally, the alignment of the section axis, which is usually required when using conventional serial sectioning techniques [11, 13], is not necessary. This advantage can increase accuracy and save much time in the observation. Moreover, because CT scanning is a non-invasive and non-destructive technique, it is possible to keep the sample intact for further observation [28, 39].

Radial variation of the grain angle

We present two image analysis methods with which to evaluate the grain angle (*δ*) of *C. camphora* from CT images (Fig. 4). Figure 4 shows the grain angle (*δ*) variation evaluated using the two methods, PIV and 2D-FFT, along the radial profile with a distinctive undulation pattern representing fluctuation of the grain angle. The fluctuation might be promoted by the inclination of longitudinal cells toward the tree axis as seen from the bark side, where a positive value represents right-handed spirals and a negative value represents

left-handed spirals. The age of the observed region was approximately 22 years according to the number of annual ring boundaries corresponding to peaks in the gray level profile (Fig. 4). Figure 4 shows that there was only one complete period of interlocked grain in the 22 annual rings. One period of interlocked grain means the length between peaks in the same direction [9], which is the 16 years from annual ring $n + 3$ to ring $n + 19$ in this case.

The radial variations of the grain angle measured using the two methods were similar. The grain angle (*δ*) of *C. camphora* ranged from $-25°$ to $16°$ when adopting 2D-FFT based on the serial tangential section and from $-22°$ to $18°$ when adopting PIV based on transverse sections. In previous work, the maximum amplitude of the *C. camphora* interlocked grain was from 10° to 15° [17]. Figure 4 shows three peaks: two peaks of left-handed grain and one peak of right-handed grain. The first peak was located in growth ring $n + 3$, the second in $n + 10$ and the third in $n + 19$. Both 2D-FFT and PIV performed well in the analysis of the grain angle variation.

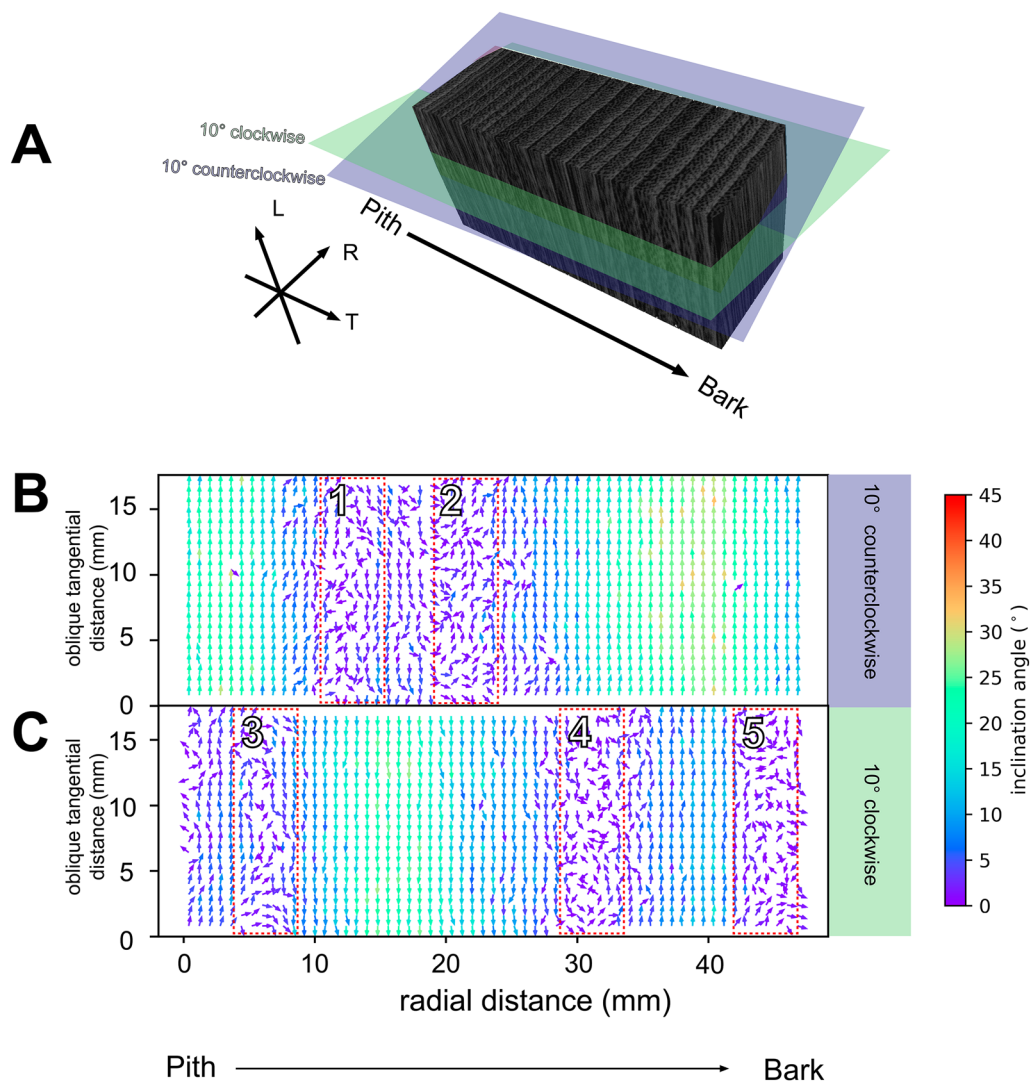Cipta *et al. Journal of Wood Science* (2022) 68:56

Page 8 of 10

Fig. 7 a Illustration of oblique transverse sections extracted from the *C. camphora* volume. Two types of oblique transverse section, with deviations of 10° counterclockwise and 10° clockwise with respect to the longitudinal axis of tree, were extracted from the *C. camphora* volume. Vector field plot showing the PIV output of the oblique transverse section inclined. **b** 10° counterclockwise and **c** 10° clockwise. The arrow color indicates the inclination angle (φ) relative to the oblique transverse section axis. Zones 1 and 2 are dominated by vessels with an inclination angle (φ) of 10° in left-handed spirals whereas zones 3, 4, and 5 are dominated by vessels with an inclination angle (φ) of 10° in right-handed spirals. Not all vectors are displayed to avoid overplotting

In this study, the maximum grain angle of *C. camphora* was 25° and 22° when measured using the 2D-FFT based on the serial tangential section and PIV based on two transverse sections, respectively. These values were lower than the maximum amplitude of 31° for the tropical species *Bagassa guianensis* [14], but higher than those for other tropical species [6, 8, 11, 13, 40, 41].

The change in grain angle had a certain intra-annual ring pattern (Fig. 4). We can see the pattern in $n+13$ annual ring to the $n+19$ annual ring. As illustrated in Fig. 5, near the earlywood, the grain angle changed with constant increment, away from the longitudinal axis. Subsequently, the grain angle increment decreases abruptly and even reverses direction in the earlywood–latewood transition zone heading into the latewood area. This variation may be related to the ability of the vessel to adjust its inclining position rapidly during secondary growth to make contact with adjacent cells [11]. Further observation is needed to confirm the intra-annual ring variation with a higher-resolution imaging technique.

Cipta *et al. Journal of Wood Science*   (2022) 68:56

Page 9 of 10

Vessel deviation in the transverse sections

The vector plot in Fig. 6b shows the variation in the grain orientation of *C. camphora* vessels in an example pair of transverse sections (Fig. 6a) with a depth difference of 500 μm. The arrows in Fig. 6b show the orientation of the tilted vessel as seen from a transverse view. Most vessels were oriented in a tangential direction (left-handed spiral or right-handed spiral) with high inclination angle. However, the vessels oriented nearly perpendicular to the transverse section (zones 1 and 2 in Fig. 6b) shows minor orientation that differed from the major orientation. The vessels were inclined towards each other, and some were moving away from each other, following the tangential direction. Some vessels tilted in the radial direction. The same phenomenon also occurred in the oblique transverse sections (Fig. 7a) that can be observed in zones 1 and 2 (Fig. 7b) with inclined vessels at 10° in left-handed spirals as well as zones 3, 4, and 5 (Fig. 7c) with inclined vessels at 10° in right-handed spirals.

Therefore, such vessel orientations continuously existed along the radial direction from the pith to bark despite the wood grain orientation changing periodically along the radial direction. This phenomenon suggests that the vessels maintain their connection to other cells by inclining at various orientations during secondary growth. The arrangement might be useful for physiological functions such as water transport in *C. camphora* trees.

Conclusion

We evaluated the interlocked grain of semi-diffuse porous hardwood *C. camphora* from images obtained using an industrial X-ray CT instrument combined with image analysis. The technique allows obtaining volumetric datasets of wood from which we are able to make virtual sections from any direction without damaging the samples. Firstly, we examined the grain angle variation from those consecutive transverse images by adopting PIV analysis to track grain displacement. Secondly, 2D-FFT analysis was performed for serial tangential sections of the same datasets. Examination of the grain angle was consistent between the PIV and 2D-FFT, with the maximum amplitude from S to Z spiral being ca. 40°. PIV can also expand our understanding of the minor orientation of vessels of the interlocked grain of *C. camphora*, which is related to the continuity of the vessel network. Such evaluation is important in the examination of mechanical properties as well as hydraulic function in woody plants.

Abbreviations
X-ray CT: X-ray computed tomography; 2D-FFT: Fast Fourier transform; PIV: Particle image velocimetry.

Supplementary Information

Author contributions
HC performed all the experiments and was a major contributor in writing the manuscript. KK supported numerical analysis throughout the study. SC aided in interpreting the results. JS edited the manuscript and supervised the work. All of the authors read and approved the final manuscript.

Availability of data and materials
The datasets used and/or analyzed in the current study are available from the corresponding author on reasonable request.

Declarations

Competing interests
The authors declare they have no competing interests.

References

1. Harris JM (1989) Spiral grain and wave phenomena in wood formation. Springer, Berlin Heidelberg
2. Hejnowicz Z, Romberger JA (1979) The common basis of wood grain figures is the systematically changing orientation of cambial fusiform cells. Wood Sci Technol 13:89–96. https://doi.org/10.1007/BF00368602
3. Krawczyszyn J, Romberger JA (1980) Interlocked grain, cambial domains, endogenous rhythms, and time relations, with emphasis on *Nyssa sylvatica*. Am J Bot 67:228–236. https://doi.org/10.1002/j.1537-2197.1980.tb07646.x
4. Brémaud I, Cabrolier P, Gril J, Clair B, Gérard J, Minato K, Thibaut B (2010) Identification of anisotropic vibrational properties of Padauk wood with interlocked grain. Wood Sci Technol 44:355–367. https://doi.org/10.1007/s00226-010-0348-0
5. Krawczyszyn J (1972) Movement of the cambial domain pattern and mechanism of formation of interlocked grain in *Platanus*. Acta Soc Bot Pol 41:443–461. https://doi.org/10.5586/asbp.1972.036
6. Hernandez RE, Almeida G (2003) Effects of wood density and interlocked grain on the shear strength of three Amazonian tropical hardwoods. Wood Fiber Sci 35:154–166
7. Ma T, Inagaki T, Tsuchikawa S (2019) Three-dimensional grain angle measurement of softwood (Hinoki cypress) using near infrared

Cipta *et al. Journal of Wood Science*   (2022) 68:56

Page 10 of 10

spatially and spectrally resolved imaging (NIR-SSRI). Holzforschung 73:817–826. https://doi.org/10.1515/hf-2018-0273

8. Coelho JCF, Vidaurre GB, da Silva JGM, de Almeida MNF, Oliveira RF, de Alcântara Segundinho PG, Alves RC, Hein PRG (2020) Wood grain angles variations in *Eucalyptus* and their relationships to physical-mechanical properties. Holzforschung 74:1089–1097. https://doi.org/10.1515/hf-2019-0131

9. Martley JF (1920) Double cross-grain. Ann Appl Biol 7:224–268. https://doi.org/10.1111/j.1744-7348.1920.tb05309.x

10. Koehler A (1931) More about twisted grain in trees. Science 73:477–477. https://doi.org/10.1126/science.73.1896.477

11. Ogata Y, Fujita M, Nobuchi T, Sahri MH (2003) Macroscopic and anatomical investigation of interlocked grain *Acacia mangium*. IAWA J 24:13–26. https://doi.org/10.1163/22941932-90000317

12. Kojs P, Włoch W, Rusin A (2004) Rearrangement of cells in storeyed cambium of *Lonchocarpus sericeus* (Poir.) DC connected with formation of interlocked grain in the xylem. Trees 18:136–144. https://doi.org/10.1007/s00468-003-0292-9

13. Ogata Y, Fujita M (2005) New anatomical method of grain angles measurement using confocal microscopy and image cross-correlation. Trees 19:73–80. https://doi.org/10.1007/s00468-004-0365-4

14. Bossu J, Lehnebach R, Corn S, Regazzi A, Beauchêne J, Clair B (2018) Interlocked grain and density patterns in *Bagassa guianensis*: changes with ontogeny and mechanical consequences for trees. Trees 32:1643–1655. https://doi.org/10.1007/s00468-018-1740-x

15. Youming X, Zehui J, Benhua F, Han L (2001) Variation of wood properties within and between camphor tree plantation and their predicting models. Sci Silvae Sin 37:92–98

16. CABI (2020) *Cinnamomum camphora* (camphor laurel) in Forestry Compendium. CAB International, Wallingford

17. Oda K, Oishi M, Ogata S, Matsumura J (2001) Formation and significance of interlocked grain in *Cinnamomum camphora l* (in Japanese). Bull Kyushu Univ For 82:11–20

18. Mertz M (2011) Wood and traditional woodworking in Japan. Kaiseisha Press, Otsu

19. Kubler H (1991) Function of spiral grain in trees. Trees 5:125–135. https://doi.org/10.1007/BF00204333

20. Kitin P, Funada R, Sano Y (2003) Three-dimensional imaging and analysis of differentiating secondary xylem by confocal microscopy. IAWA J 24:211–222. https://doi.org/10.1163/22941932-90001590

21. Bhat KV, Bhat KM (1983) Anatomical changes associated with interlocked grain in *Anacardium occidentale* L. IAWA J 4:179–182. https://doi.org/10.1163/22941932-90000410

22. Collings DA, Thomas J, Dijkstra SM, Harrington JJ (2021) The formation of interlocked grain in African mahogany (*Khaya* spp.) analysed by X-ray computed microtomography. Tree Physiol 41:1542–1557. https://doi.org/10.1093/treephys/tpab020

23. Spicer R (2016) Variation in angiosperm wood structure and its physiological and evolutionary significance. In: Groover A, Cronk Q (eds) Comparative and evolutionary genomics of angiosperm trees. Springer International Publishing, Cham, pp 19–60

24. Kitin PB, Fujii T, Abe H, Funada R (2004) Anatomy of the vessel network within and between tree rings of *Fraxinus lanuginosa* (Oleaceae). Am J Bot 91:779–788. https://doi.org/10.3732/ajb.91.6.779

25. Brodersen CR (2013) Visualizing wood anatomy in three dimensions with high-resolution X-ray micro-tomography (μCT)—a review –. IAWA J 34:408–424. https://doi.org/10.1163/22941932-00000033

26. Thomas J, Dijkstra SM, Harrington JJ, Collings DA (2022) Induction of compression wood inhibits development of spiral grain in radiata pine. IAWA J (published online ahead of print 2022): https://doi.org/10.1163/22941932-bja10088

27. Stock SR (2008) Recent advances in X-ray microtomography applied to materials. Int Mater Rev 53:129–181. https://doi.org/10.1179/174328008X277803

28. Kobayashi K, Akada M, Torigoe T, Imazu S, Sugiyama J (2015) Automated recognition of wood used in traditional Japanese sculptures by texture analysis of their low-resolution computed tomography data. J Wood Sci 61:630–640. https://doi.org/10.1007/s10086-015-1507-6

29. Bengough AG, Hans J, Bransby MF, Valentine TA (2009) PIV as a method for quantifying root cell growth and particle displacement in confocal images. Microsc Res Tech 73:27–36. https://doi.org/10.1002/jemt.20749

30. Mittelstaedt E, Davaille A, van Keken PE, Gracias N, Escartin J (2010) A noninvasive method for measuring the velocity of diffuse hydrothermal flow by tracking moving refractive index anomalies. Geochem Geophys Geosystems 11:Q10005. https://doi.org/10.1029/2010GC003227

31. Wong AD, Searson PC (2014) Live-cell imaging of invasion and intravasation in an artificial microvessel platform. Cancer Res 74:4937–4945. https://doi.org/10.1158/0008-5472.CAN-14-1042

32. Huertas-Tato J, Aler R, Rodríguez-Benítez FJ, Arbizu-Barrena C, Pozo-Vázquez D, Galván IM (2018) Predicting global irradiance combining forecasting models through machine learning. In: de Cos Juez FJ, Villar JR, de la Cal EA, Herrero Á, Quintián H, Sáez JA, Corchado E (eds) Hybrid artificial intelligent systems. Springer International Publishing, Cham, pp 622–633

33. Schlüter S, Leuther F, Vogler S, Vogel H-J (2016) X-ray microtomography analysis of soil structure deformation caused by centrifugation. Solid Earth 7:129–140. https://doi.org/10.5194/se-7-129-2016

34. Python Software Foundation (2016) Python version 3.5. https://www.python.org/. Accessed 04 Apr 2017

35. Liberzon A, Lasagna D, Aubert M, Bachant P, Jakirkham, Ranleu, Borg J, Dallas C (2017) Openpiv/Openpiv-Python: bug fixes from 0.20.8 due to Python 3 division and from range(0,0) to range(0,1). Zenodo. https://doi.org/10.5281/zenodo.1004649. Accessed 23 Apr 2018

36. Taylor ZJ, Gurka R, Kopp GA, Liberzon A (2010) Long-duration time-resolved PIV to study unsteady aerodynamics. IEEE Trans Instrum Meas 59:3262–3269. https://doi.org/10.1109/TIM.2010.2047149

37. Liu Z-Q (1991) Scale space approach to directional analysis of images. Appl Opt 30:1369. https://doi.org/10.1364/AO.30.001369

38. Schindelin J, Arganda-Carreras I, Frise E, Kaynig V, Longair M, Pietzsch T, Preibisch S, Rueden C, Saalfeld S, Schmid B, Tinevez JY, White DJ, Hartenstein V, Eliceiri K, Tomancak P, Cardona A (2012) Fiji: an open-source platform for biological-image analysis. Nat Methods 9:676–682. https://doi.org/10.1038/nmeth.2019

39. Steppe K, Cnudde V, Girard C, Lemeur R, Cnudde JP, Jacobs P (2004) Use of X-ray computed microtomography for non-invasive determination of wood anatomical characteristics. J Struct Biol 148:11–21. https://doi.org/10.1016/j.jsb.2004.05.001

40. Thinley C, Palmer G, Vanclay JK, Henson M (2005) Spiral and interlocking grain in *Eucalyptus dunnii*. Holz Als Roh- Werkst 63:372–379. https://doi.org/10.1007/s00107-005-0011-x

41. Nistal França FJ, Filgueira Amorim França TS, Vidaurre GB (2020) Effect of growth stress and interlocked grain on splitting of seven different hybrid clones of *Eucalyptus* grandis × *Eucalyptus urophylla* wood. Holzforschung 74:917–926. https://doi.org/10.1515/hf-2019-0209

Publisher's Note
Springer Nature remains neutral with regard to jurisdictional claims in published maps and institutional affiliations.